International Journal of Engineering Research & Technology (IJERT)
ISSN: 2278-0181
Vol. 11 Issue 11, November-2022

Structural and Optical Properties of $ZnTiO_3$ Nanoparticles Synthesized by Hydrothermal Method

M. Vijaya Saritha[1], S Dastagiri[1], M. V. Lakshmaiah[1*], V. Ramesh Kumar[2], K.E.Supriya[1], and G. Pakardin[2]
[1]Department of Physics, Sri Krishnadevaraya University, Anantapuramu, A.P, India.
[2]Department of Physics, PSC & KVSC Govt. Degree College, Nandyal, A.P, India.
[3]Department of Physics, Govt. Degree College (A), YSR Kadapa, A.P, India.

Abstract:- **$ZnTiO_3$ is a promising wide-energy band gap semiconductor material because of its current and potential uses in catalysts, microwave insulators, luminous materials, nonlinear optics, solar cells, and gas sensors. In the present work, $ZnTiO_3$ nanoparticles were synthesized by hydrothermal method. The structural properties and parameters have been investigated by using X-ray diffraction (XRD). The XRD results raveled that the particle attributed high phase purity, and good crystalline. The structure of $ZnTiO_3$ nanoparticles found cubic spinel phase and using the Scherrer equation the average crystallite size was calculated as 31.74 nm. The X-ray peak broadening analysis was used to evaluate the crystalline sizes and lattice strain by the Williamson-Hall (W-H) analysis. The functional group information conforms to the $ZnTiO_3$ nanoparticles. The FE-SEM images showed the particle shape spherical with partial agglomeration. Furthermore, the optical band gap (E_g) was determined using UV–Visible spectra.**

Keywords: XRD, FTIR, UV-Vis, Hydrothrmal Method and Optical band gap

1. INTRODUCTION

The development of nanomaterials has been strongly pursued due to their unique features such as electronic, chemical, mechanical, magnetic, and optical properties that differ from bulk materials [1–11]. Size-dependent properties are observed such as surface plasmon resonance in some metal particles, quantum confinement in semiconductor particles, and superparamagnetism in magnetic materials. Among the different nanomaterials, perception of the behavior of ferroelectric materials at the nanoscale is important for the growth of molecular electronics. Indeed, perovskite-phase mixed-metal oxides are significant for their advantageous electrostrictive, pyroelectric, piezoelectric, electro-optic and dielectronic properties with corresponding applications in the electronics industry for high-k-dielectrics, actuators, and transducers [12, 13]. Among perovskite-phase mixed-metal oxides, $ZnTiO_3$ has been reported to have superior electrical properties that are sufficient for applications towards microwave dielectrics [14]. Furthermore, $ZnTiO_3$ is an effective photocatalyst because this compound is categorized in a group of coupled photocatalysts that can help to enhance the photocatalytic activity of TiO_2 through reducing recombination process and change band gap to enhance the optical response in the UV to the visible light range [15, 16]. Pure h- $ZnTiO_3$ represents superior dielectric properties in the microwave range. Many reports have been made to produce pure $ZnTiO_3$ powders and ceramics. But the synthesis of pure $ZnTiO_3$ from a mixture of ZnO and TiO2 with a molar ratio of 1 was not successful. There are various problems with the synthesis of pure $ZnTiO_3$ powders by the solid-state reaction method such as large particle size, a limited degree of chemical homogeneity, high temperature, and long range of diffusion distance. In the past two decades, the sol-gel route has been successfully used for the preparation of ceramics, thin films, fibers, and glasses; this method has various advantages such as low calcination temperature, low cost, chemical homogeneity, and easy component adjustment. Besides, the sol-gel route is one of the methods for the synthesis of nanomaterials [17, 18]. Here, $ZnTiO_3$ nanostructures were synthesized by an unusual sol-gel method. Utilizing new and smaller number chemical materials in addition to a simple procedure is the characteristic benefit of this method in assessment to the other reports [19, 20]. In this paper, $ZnTiO_3$ nanoparticles were successfully synthesized by hydrothermal method. The products were characterized by various analyses such as XRD, SEM, TEM, EDS, FT-IR, and UV-Vis spectroscopy.

2. EXPERIMENTAL

To synthesize the ZT nanoparticles, the starting materials were chosen as Zn $(NO_3)_2$ $6H_2O$ and TiO_2 (each of 99.9% purity, Sigma-Aldrich). These precursors were mixed after taking their stoichiometric ratio. The whole mixed precursors were transferred to a glass beaker. Furthermore, distilled water was added to the precursors in a ratio of 1:4 (mixed precursors (gm): distilled water (ml)) and the resultant solution was kept on a magnetic stirrer. A stirring rate of 500 rpm was maintained to stir the solution. Later NaOH solution was slowly added, and the pH value reached 11. Furthermore, this solution was transferred to a 500 ml Teflon bowl

International Journal of Engineering Research & Technology (IJERT)
ISSN: 2278-0181
Vol. 11 Issue 11, November-2022

inserted in an autoclave. The sealed autoclave was kept in a hot-air oven at an operating temperature of 150°C/8 hours. After completion of the reaction, the autoclave was slowly cooled to room temperature. The final $ZnTiO_3$ nanoparticles were removed from the Teflon-lined autoclave and washed with acetone and distilled water several times until the pH was reduced to 7. Later it was heated at 60°C/2 hour. The final ZT new particles were removed and characterized for various characterized techniques such as the X-ray diffraction method, field emission scanning, and transition electron microscopy. In addition, the Fourier transform infrared spectroscopy (FTIR), and UV-Visible techniques were used to find the presence of metal oxide bands and the optical energy band gap.

3. *Results and discussion*

3.1. XRD analysis

The diffraction pattern of ZT nanoparticles is depicted in Figure 1. It can be seen that the Zinc titanate (ZT) nanoparticles exhibit the cubic perovskite structure about the reflection planes as indicated in Figure 1. These reflection planes are in good agreement with the Joint Committee on Powder Diffraction Standards (JCPDS) data of file number: 39–0190. Amongst these planes, the 211 planes at 25.3579° revealed the maximum intensity. No secondary peaks are observed in the ZT structure. The average crystallite size (D_a) is evaluate with the help of the average full-width at half maxima (FWHM) of reflection planes using the Debye-Scherrer equation [22],

$$D_a = (k\lambda) / \beta Cos\theta \qquad (1)$$

Where β is full-width half maxima, λ is the wavelength of CuK_α radiation (0.15406 nm), θ is the diffraction angle, and "k" is a numerical constant that is equal to 0.9 for a spherical atom. The results are repeated in Table 1. It is clear from the table that the average crystal size is D_a is calculated to be 31.74 nm.

Figure 2, depicts the variation of D_a and micro-strain as a function of diffraction angle. It is very clear from the figure that there exists a reciprocal relationship between micro-strain and D_a. Similar kinds of observations were previously reported in the literature [23]. In addition, the lattice constant (a) is calculated after finding the inter-planar spacing (d) and miller indices (hkl) by using the following formula [23]:

$$a = d\,(h^2+k^2+l^2)^{1/2} \qquad (2)$$

The lattice parameter is found to be 8.391 Å. The X-ray density (D_x) is evaluated using the formula Z M.W/NV, where "Z" is the number of molecules per unit cell (Z = 8), "M.W" is the molecular weight of the composition, "N" is Avogadro's number (6.023 x 10^{23}), and "V" is the Volume [23]. The calculated numerical value of D_x is 3.517 g/cm^3 of ZT nanoparticles [24]. This may be attributed to the high homogeneity of prepared ZT nanoparticles. Moreover, the structural parameters such as inter-planer spacing (d), FWHM, micro-stain (ε), miller indices (h k l), and dislocation density (ρ) are listed in Table 1 as a function of diffraction angle.

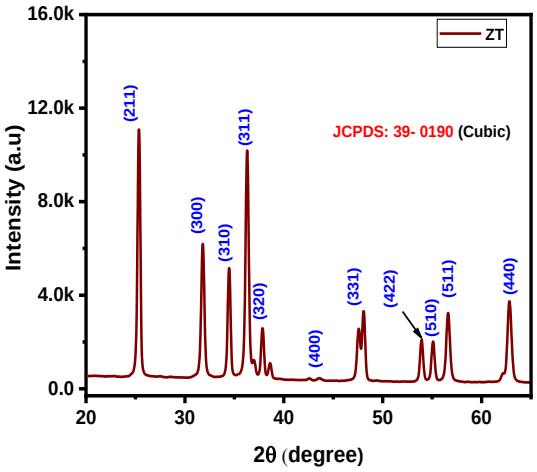

Fig. 1. The diffraction pattern of ZT nanoparticles.

Table 1. The data on structural and physical parameters of ZT nanoparticles

2θ (°)	FWHM β (°)	d (Å)	ε	D_a (nm)	hkl	ρ (m^{-2})
25.3579	0.1861	3.509	0.003609	43.7528	211	5.22E+14
31.8093	0.2630	2.810	0.004027	31.4075	300	1.01E+15
34.4708	0.2090	2.599	0.002940	39.7828	310	6.32E+14
36.2927	0.2743	2.473	0.003652	30.4756	311	1.08E+15
37.8497	0.2182	2.375	0.002776	38.4871	320	6.75E+14
47.8762	0.8057	1.898	0.007919	10.7881	331	8.59E+15
53.9284	0.2442	1.698	0.002095	36.4878	422	7.51E+14
55.0872	0.2501	1.665	0.002092	35.8263	510	7.79E+14
56.6124	0.3383	1.624	0.002741	26.6667	511	1.41E+15
62.8195	0.3924	1.478	0.002803	23.7221	440	1.78E+15

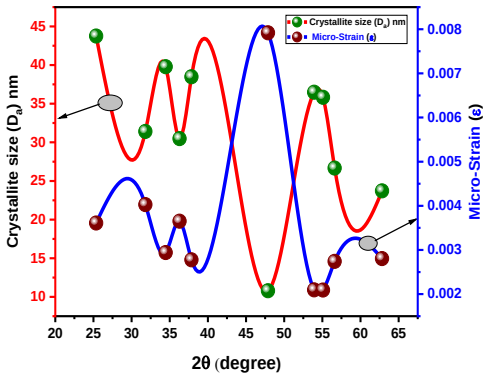

Figure 2. The variation of micro-strain and D_a of ZT nanoparticles

The inter-planer spacing is decreasing with an increase of 2θ angle. In addition, the dislocation density is a parameter that evaluates the defects per unit area of the sample. The smaller value of ρ indicates the low porous structure of ZT nanoparticles and vice versa. In the current study, the

International Journal of Engineering Research & Technology (IJERT)
ISSN: 2278-0181
Vol. 11 Issue 11, November-2022

average ρ is ~ 1.72 × 10^{15} m^{-2}. The micro-strain at an average of all diffraction angles is noticed as 0.00346. The specific surface area (S) is a significant physical parameter for nanoparticles and is computed using the relation $6000/D_aD_x$, where the symbols have their usual meaning [25]. In this study, the S is achieved to be ~ 54 m^2/g. This kind of high value of S can be attributed to the smallest value of D_a when compared with bulk materials. This larger S value in turn affects the electrical, optical, and morphological properties of nanoparticles.

Williamson–Hall (W–H) plot (as shown in Figure 3) is drawn for βcosθ versus 4sinθ to evaluate micro-strain (ε) and crystallite size (D_p) using the following relation [26],

$$\beta\,Cos\theta = (0.9\lambda/D) + 4\varepsilon\,Sin\theta \qquad (3)$$

where the slope of a straight line offers micro-strain while D_a is associated with to intercept parameter. This provides the correlation between strain and size of the crystallite. The results from W–H plot express that the stain (0.00131) is almost consistent with the Scherrer strain from the diffraction pattern. The average D_a is of the order of 61.08 nm which is almost in agreement with the Scherrer size.

3.2. Surface morphology

The surface morphology of ZT nanoparticles is analyzed by a field emission scanning electron microscope (FESEM) and a High-Resolution transmission electron microscope (HRTEM). The FESEM photographs of ZT nanoparticles are shown in Figure 4(a). From Figure 4(a), it is noticed that ZT shows well-defined spherical shapes and rods. The grain size (G_a) is determined using the linear intercept method [25]

$$G_a = \frac{3\,L}{2MN} \qquad (4)$$

where "L" is the line length, "N" is the number of grains intercepting the test line, and "M" is the magnification. The average grain size (G_a) is 135.03 nm. This confirms the presence of microspheres and rods. The energy dispersive X-ray analyzer (EDAX) (Figure 4(c)) reveals the presence of Zn, Ti, and O elements. HRTEM generally provides information about the existence of nanoparticles. The HRTEM images of ZT nanoparticles are shown in Figure 4(b). It is seen from Figure 4(b) that all ZT nanoparticles are spherical in shape. The average particle size is 112.57 nm. In HRTEM images a weak agglomeration is identified.

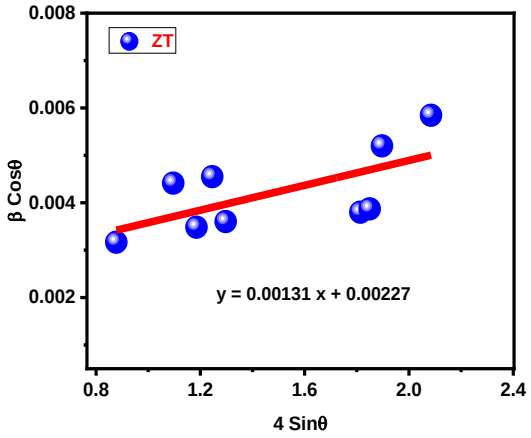

Figure 3. The W–H plot of ZT nanoparticles

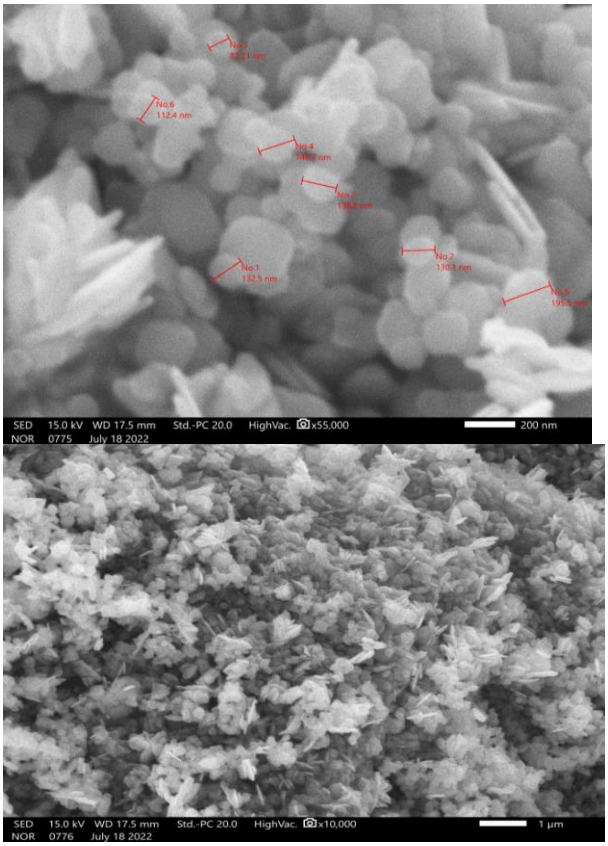

Figure 4. (a) The FESEM photos of ZT nanoparticles

International Journal of Engineering Research & Technology (IJERT)
ISSN: 2278-0181
Vol. 11 Issue 11, November-2022

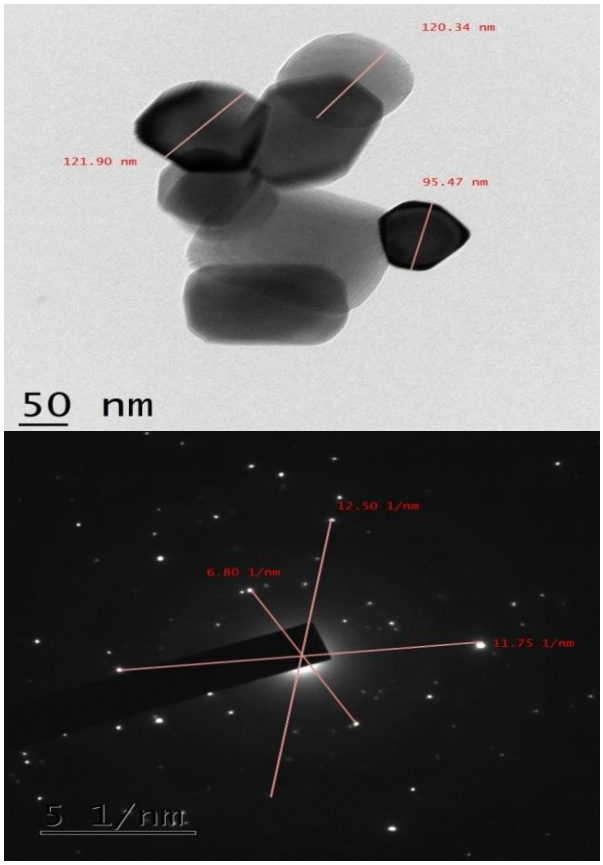

Figure 4. (b) The HRTEM with SAED photos of ZT nanoparticles.

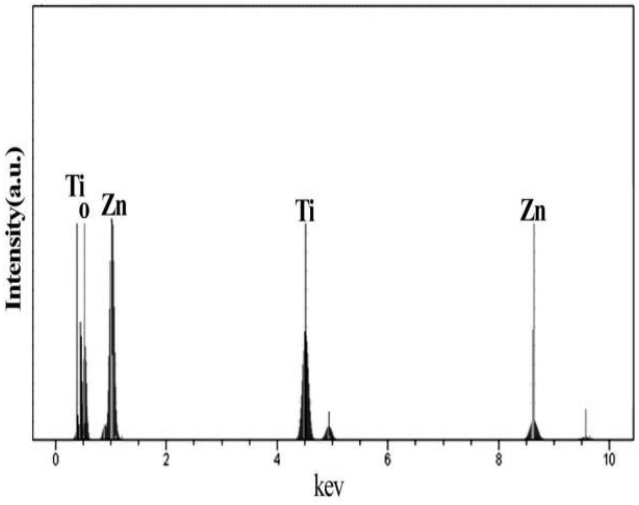

Figure 4. (c) The EDAX of ZT nanoparticles.

3.3 Optical Properties

3.3.1. FTIR analysis

In order to study the characteristic vibration bands corresponding to different bonds, the FT-IR spectra (Fig. 5) is used in the spectral range of 400–4000 cm^{-1}. It is well known that the characteristic vibration bands corresponding to metal-oxygen bonds be in the range of 400–700 cm^{-1}. As seen from the spectrum, peaks 464.84 cm^{-1} and 634.58 cm^{-1} are the characteristic bands of ZnTiO3, corresponding to the stretching vibration of the Zn–O and Ti–O bond [26]. Also, in the bonds at 1529.41–2090.28 cm^{-1} and 2337.43–3742.81 cm^{-1} wave number range, the peaks were tailored owing to the O–H stretching and bending vibrations of H_2O molecules absorbed by the ZT nanoparticles [27]. So, the FT-IR spectrum confirms that ZnTiO3 nanostructures were produced according to appeared peaks.

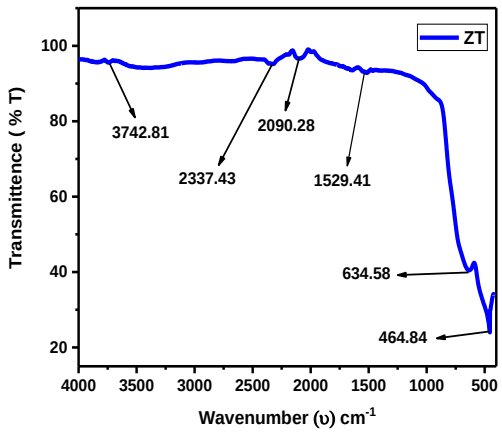

Figure 5. The FTIR spectra of ZT nanoparticles

3.3.2. UV-visible spectral analysis

The room temperature UV–Vis absorption spectra of ZnTiO3 nanoparticles were also measured in the range of 200–1600 nm. Fig. 6 (a) shows the diffuse reflection adsorption spectra (DRS) of the ZnTiO3 nanoparticles at room temperature. The figure indicates that the ZnTiO3 nanoparticles show absorption maxima at 312.04nm, the direct optical band gap estimated from the absorption spectra of the $ZnTiO_3$ nanoparticles is shown in Fig. 6(b). An optical band gap is obtained by plotting $(\alpha h\upsilon)^2$ vs $h\upsilon$ where α is the absorption coefficient and $h\upsilon$ is photon energy. Extrapolation of the linear portion at $(\alpha h\upsilon)^2 = 0$ gives the band gaps of 3.19 eV for perovskite ZnTiO3 nanoparticles. The optical band gap of ZnTiO3 nanoparticles is smaller than those of the bulk ZnTiO3 (band gap 3.70 eV) [29].

International Journal of Engineering Research & Technology (IJERT)
ISSN: 2278-0181
Vol. 11 Issue 11, November-2022

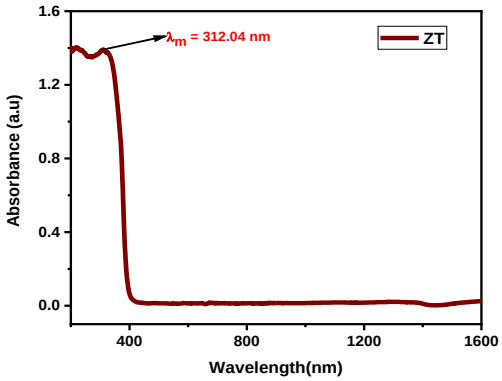

Figure 6(a). The absorption spectra of ZT nanoparticles.

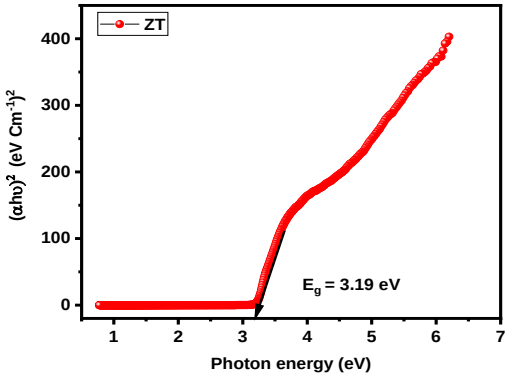

Figure 6(b). The "αhv" versus photon energy of ZT nanoparticles.

4. CONCLUSIONS

The hydrothermal method in comparison to other synthetic methods of nanoparticle preparation has many advantages, for example: simple, available, and inexpensive. In this work, we have prepared the $ZnTiO_3$ nanoparticles by hydrothermal method. A systematic study on the structural, morphological, and optical properties of $ZnTiO_3$ nanoparticles was carried out using various analyses. FESEM images reveal that the $ZnTiO_3$ have a mean particle size of about 135.03, with spherical-like shapes and rods. The average particle size was 112.57 nm using HRTEM images. The band gap was 3.19 eV estimated by UV-vis spectroscopy.

ACKNOWLEDGMENT

My special thanks go to SRMIST consultancy, SRM University, Chennai for providing me the necessary characterizations (XRD, FTIR, and UV-Vis), SEM with EDAX providing Yogi Vemana University, YSR Kadapa, and HRTEM with SAED providing STIC, Cochin University, Kerala.

REFERENCES:

[1] Y. Xiong, B. Wang, W. Hu, L. Dai, Facile synthesis and characterization of erythrocyte-like Y-doped $PbWO_4$ mesocrystals and their photocatalytic activity, Materials Characterization 105 (2015) 24–29.

[2] M. Dadkhah, M. Salavati-Niasari, N. Mir, Synthesis and characterization of TiO_2 nanoparticles by using new shape controllers and its application in dye-sensitized solar cells, Journal of Industrial and Engineering Chemistry, 20: (2014) 4033-4039

[3] M. Sabet, M. Salavati-Niasari, Deposition of cadmium selenide semiconductor nanostructures on TiO_2 surface via different chemical methods and investigation of their effects on dye-sensitized solar cell efficiency, Materials Science in Semiconductor Processing, 27 (2014) 610-619.

[4] N. Mir, M. Salavati-Niasari, TiO_2 nanoparticle aggregations prepared by nitro-functionalized tripodal ligand as promising candidates for dye-sensitized solar cells, Materials Science in Semiconductor Processing, 27 (2014) 695-702.

[5] M. Sabet, M. Salavati-Niasari, O. Amiri, Using different chemical methods for deposition of CdS on TiO_2 surface and investigation of their influences on the dye-sensitized solar cell performance, Electrochimica Acta, 117 (2014) 489-504.

[6] N. Mir, M. Salavati-Niasari, Photovoltaic properties of corresponding dye-sensitized solar cells: Effect of active sites of growth controller on TiO_2 nanostructures, Solar Energy, 86 (2012) 3389-3397.

[7] M. Masjedi, N. Mir, E. Noori, T. Gholami, M. Salavati-Niasari, Effect of Schiff base ligand on the size and the optical properties of TiO_2 nanoparticles, Superlattices and Microstructures, 62 (2013) 21-30.

[8] S. Mandizadeh, M. Bazarganipour, A low-cost and eco-friendly viable approach for green synthesis of barium hexaferrite nanostructures using palm oil, M. Salavati-Niasari, Ceramics International, 40 (2014) 15680-15685.

[9] K.J. Klabundl, Nanoscale Materials in Chemistry, Wiley-Interscience, New York, 2001 51-55.

[10] A.P. Alivisatos, Semiconductor clusters, nanocrystals, and quantum dots, Science, 271 (1996) 933-937.

[11] M. Nirmal, L.E. Brus, Luminescence photophysics in semiconductor nanocrystals, Acc. Chem. Res. 32 (1999) 407-414.

[12] N.A. Hill, Why Are There so Few Magnetic Ferroelectrics, J. Phys. Chem. B 104 (2000) 6694-6709.

[13] A.J. Millis, Lattice effects in magnetoresistive manganese perovskites, Nature, 392 (1998) 147-150.

[14] S. Ke, X. Cheng, Q. Wang, Y. Wang, Preparation ofaphotocatalyticTiO2/ZnTiO3 coating on glazed ceramic tiles, Ceramics Internationa l40 (2014) 8891–8895.

[15] H. Xu, S. Ouyang, L. Liu, P. Reunchan, N. Umezawa, J. Ye, Recent advances in TiO_2-based photocatalysis, J. Mater. Chem. A, 2 (2014) 12642-12661.

[16] C.F. Shih, W.M. Li, M.M. Lin, K.T. Hung, Microelectrode Study of Pore Size, Ion Size, and Solvent Effects on the Charge/Discharge Behavior of Microporous Carbons for Electrical Double-Layer Capacitors, J. Electrochemical Soc. 156 (2009) 7-12.

[17] F. Ansari, F. Soofivand, M. Salavati-Niasari, Utilizing maleic acid as a novel fuel for synthesis of $PbFe_{12}O_{19}$ nanoceramics via sol–gel auto-combustion route, Materials Characterization, 103 (2015) 11-17.

[18] S. Mandizadeh, F. Soofivand, M. Salavati-Niasari, Sol–gel auto combustion synthesis of $BaFe_{12}O_{19}$ nanoceramics by using carbohydrate sugars as a novel reducing agent, Advanced Powder Technology 26 (2015) 1348-1354.

[19] S.F. Wang, F. Gu, M.K. Lu, C.F. Song, S.W. Liu, D. Xu, D.R. Yuan, Preparation and characterization of sol–gel derived $ZnTiO_3$ nanocrystals, Materials Research Bulletin 38 (2003) 1283-1288.

[20] Y.S. Chang, Y.H. Chang, I.G. Chen, G.J. Chen, Y.L. Chai, Synthesis and characterization of zinc titanate nano-crystal powders by sol–gel technique, Journal of Crystal Growth 243 (2002) 319–326.

[21] W.G. Klemperer, S.D. Ramamurthy, Molecular growth pathways in silica sol–gel polymerization, vol.121, Pittsburgh, PA,. in: C.J. Brinker, D.E. Clarke, D.E. Ulrich, Material Research Society Symposium Proceedings, (1988) 1-33.

International Journal of Engineering Research & Technology (IJERT)
ISSN: 2278-0181
Vol. 11 Issue 11, November-2022

[22] Maddaiah M, Naidu KCB, Rani DJ, et al. Synthesis and characterization of CuO-doped SrTiO3 ceramics. J Ovonic Res. 2015; 11:99–106.
[23] Chandra Babu Naidu K, Madhuri W. Microwave processed NiMg ferrite: studies on structural and magnetic properties. J Magn Magn Mater. 2016;420:109–116.
[24] Reddy VN, Babu Naidu KC, Subbarao T. Structural, optical and ferroelectric properties of BaTiO3 ceramics. J Ovonic Res. 2016;12:185–191.
[25] Chandra Babu Naidu K, Madhuri W. Microwave assisted solid state reaction method: investigations on electrical and magnetic properties NiMgZn ferrites. Mater Chem Phys. 2016; 181:432–443.
[26] H.Q. Fan, H.E. Kim, Japanese Journal of Applied Physics, 41 (2002) 6768– 6772
[27] Tai Duc Tran & Moon Il Kim, Organic-Inorganic Hybrid Nanoflowers as Potent Materials for Biosensing and Biocatalytic Applications. Bio Chip J. 12, 268–279 (2018)